ACS chemical biology

Articles

Cite This: ACS Chem. Biol. 2020, 15, 234−242

pubs.acs.org/acschemicalbiology

A Unique Conformational Distortion Mechanism Drives Lipocalin 2 Binding to Bacterial Siderophores

Xiaojing Huang,[†] Sladjana Slavkovic,[†] Erfei Song,[‡] Amy Botta,[‡] Banafsheh Mehrazma,[†] Cristina Lento,[†] Philip E. Johnson,[†] Gary Sweeney,[‡] and Derek J. Wilson*[,†,§]

[†]Department of Chemistry, [‡]Department of Biology, and [§]Center for Research in Mass Spectrometry, York University, Toronto, Ontario M3J 1P3, Canada

Supporting Information

ABSTRACT: Lcn2 is a host defense protein induced via the innate immune response to sequester iron-loaded bacterial siderophores. However, excess or prolonged elevation of Lcn2 levels can induce adverse cellular effects, including oxidative stress and inflammation. In this work, we use Hydrogen−Deuterium eXchange (HDX) and Isothermal Titration Calorimetry (ITC) to characterize the binding interaction between Lcn2 and siderophores enterobactin and 2,3-DHBA, in the presence and absence of iron. Our results indicate a rare "Type II" interaction in which binding of siderophores drives the protein conformational equilibrium toward an unfolded state. Linking our molecular model to cellular assays, we demonstrate that this "distorted binding mode" facilitates a deleterious cellular accumulation of reactive oxygen species that could represent the molecular origin of Lcn2 pathology. These results add important insights into mechanisms of Lcn2 action and have implications in Lcn2-mediated effects including inflammation.

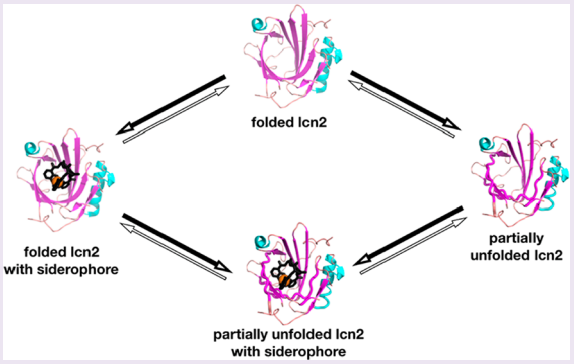

Lipocalin 2 (Lcn2) is a mammalian bacteriostatic protein whose primary function is to limit bacterial iron acquisition by binding iron-loaded siderophores and transferring them into host cells. It is induced and secreted by neutrophils as part of the innate immune response.[1,2] Circulating Lcn2 levels are found to be elevated in a host of chronic conditions associated with inflammation, such as obesity and diabetes, and are thought to contribute to disease pathogenesis.[3,4] Despite this, Lcn2 does not mediate biological effects via a classic receptor signal transduction pathway, and the precise molecular mechanisms of action remain to be fully elucidated. Recent studies have shown that Lcn2 mediated binding and transport of iron-loaded siderophores into mammalian cells can elicit substantial and varied cellular responses.[3,5]

Lcn2 has a classic β-barrel structure of the lipocalin family with eight antiparallel β-sheets, and an unusually large and polar ligand-binding cavity or calyx.[6,7] Due to its structural similarity to other lipocalin family members, Lcn2 was initially proposed to be a carrier protein for small lipophilic compounds.[8] Interactions with a variety of lipophilic substances have been reported, including N-formyl-Met-Leu-Phe, leukotriene B4, platelet-activating factor, cholesteryl oleate, retinol, and retinoic acid.[6,9] However, all the proposed ligands above have weak binding affinities and/or exhibit poor docking in the calyx.[1]

In the search for the "true" native ligand of Lcn2, the cocrystallization of Lcn2 with enterobactin (Ent) marked a critical advance.[10] In their structural study, Goetz et al. describe the interaction between Ent and Lcn2 through three positively charged residues inside the calyx. Ent acts as an iron chelator, resulting in a "holo" complex corresponding to Lcn2-Ent-Fe. The characterization of this complex validated the role for Lcn2 as an antimicrobial protein that limits bacterial growth by preventing iron acquisition.[10,11] Indeed, Lcn2 knockout mice are more susceptible to bacterial infection.[12] Thus, the available literature suggests that Lcn2 plays a pivotal role in the innate immune system.[13] After identification of the Lcn2-Ent-Fe interaction, a range of related microbial siderophores were scanned for Lcn2 binding. Both a catecholate and a precursor in Ent biosynthesis, 2,3-dihydroxybenzoic acid (DHBA) showed a high affinity for Lcn2 in the presence of iron.[14]

Outside of acute infection, the physiological role of Lcn2 is closely related to inflammation, although the exact mechanistic pathways remain obscure. Under certain conditions, such as inflammatory bowel disease, Lcn2 released by colonic epithelial cells prevents inflammation by strengthening phagocytic bacterial clearance.[15] On the other hand, seemingly contradictory evidence implies a pro-inflammatory effect of Lcn2 in low-grade bowel inflammation.[16] Under chronic neuroinflammatory conditions, Lcn2 promotes inflammation

Received: October 11, 2019
Accepted: October 15, 2019
Published: October 15, 2019

DOI: 10.1021/acschembio.9b00820
ACS Chem. Biol. 2020, 15, 234−242

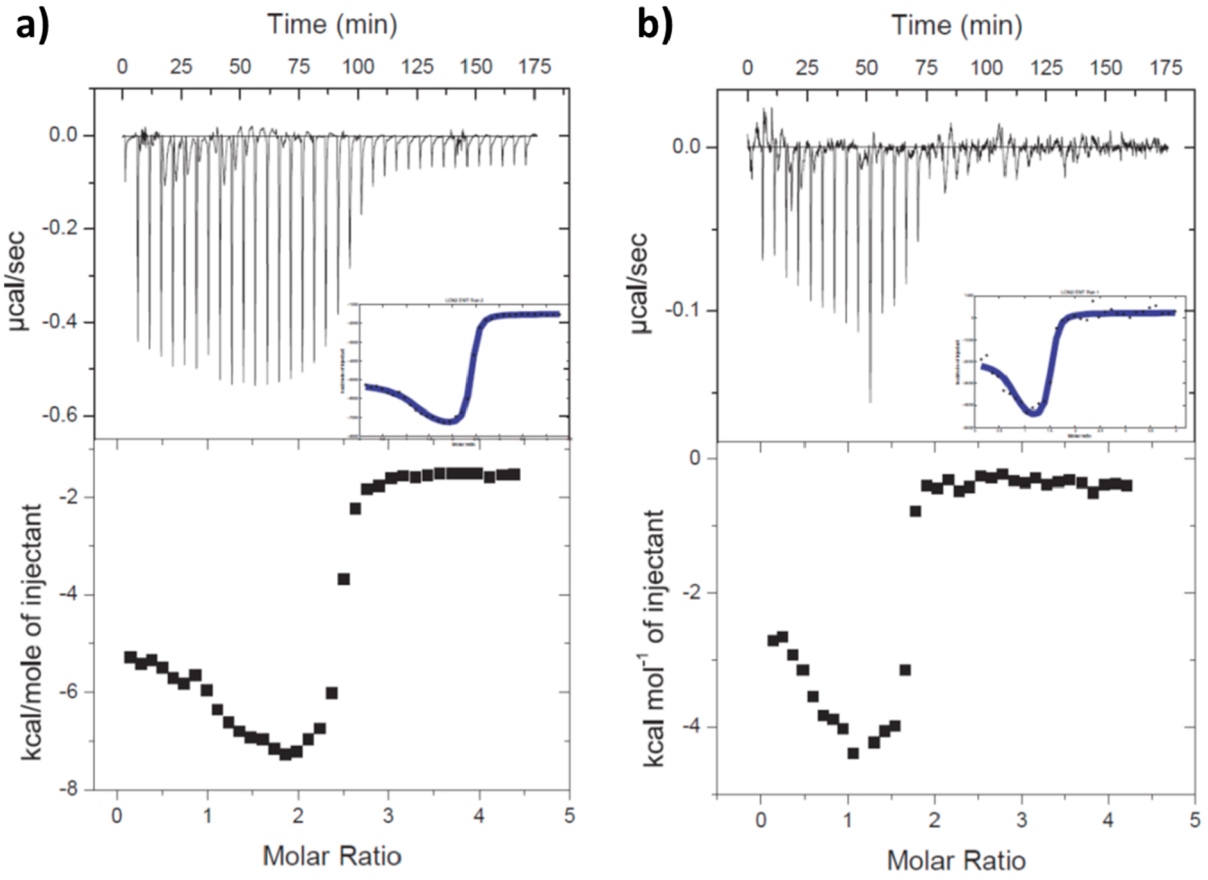

Figure 1. ITC thermograms of Ent binding by Lcn2. (a) 40 μM Lcn2. (b) 12 μM Lcn2. In both cases, the data cannot be fit using a single event model, but can be fit to a sequential muti-event model (insets).

through the TNFα pathway.[17] In obese and diabetic models, which are considered prolonged weak inflammation, Lcn2 has a pro-inflammatory aspect as well.[4,18,19] That Lcn2 expression is positively regulated by pro-inflammatory cytokines, like NF-κB, also supporting a proinflammation hypothesis.[20]

To reconcile these contradictory roles, a dual mechanism of Lcn2 activity has been suggested.[21] On the anti-inflammatory side, a recent report suggests that when free Lcn2 (apo-Lcn2) enters cells and accumulates, it can attenuate iron or siderophore induced reactive oxygen species (ROS) production and enhance cell survival.[22] However, when Lcn2 complexed with iron-loaded siderophore (holo-Lcn2) enters cells, it promotes cell death via ROS production.[22] Therefore, the presence or absence of siderophores in the extracellular environment is likely a critical factor in determining Lcn2 function in both microbe-induced and sterile inflammation.[23−26] In the current study, we aim to shed light on the molecular basis of Lcn2 physiology by probing the thermodynamic, structural, and dynamic aspects of Lcn2−siderophore interactions. Physiological effects that result from the observed "strained" binding mode are then probed via ROS-sensing cell-based assays.

RESULTS AND DISCUSSION

Lcn2-Siderophore Binding Is Not a Single-Event Process. To understand the thermodynamics of Lcn2 siderophore engagement, we titrated Ent into Lcn2 in the absence of iron in a series of Isothermal Titration Calorimetry (ITC) measurements. Iron-free Ent was the only siderophore that gave interpretable results, with Fe-Ent being too low in K_d and DHBA giving an exceedingly complex thermogram that indicated weak binding, but could not be fit to a low-parameter model. For Ent-Lcn2 complexation, the U-shaped curve could only be described using a sequential, minimum two-event model (Figure 1). While these results unambiguously indicate a process that involves more than one thermodynamically favorable phase, any quantitative interpretation of the data would be largely speculative, since there is at least one phase that cannot be assigned to a known physical process.

The "secondary" phase in the ITC curve could have a number of causes, including a second binding site,[27,28] ligand-induced dimerization,[29] or perturbation of protein folding/unfolding equilibrium.[30,31] As the crystal structure of the human homologue NGAL reveals, Lcn2 only has one cup-shaped cavity suitable for Ent.[7] Thus, Lcn2 is unlikely to specifically accommodate a second Ent. On the other hand, Lcn2 has been reported to be isolated from neutrophils and crystallized as homodimers.[32,33] To investigate further, we implemented a series of native MS-based analyses.

Siderophore Biding Does Not Induce Lcn2 Dimerization. We conducted electrospray ionization (ESI) native mass spectrometry (MS) on various siderophore-Lcn2 pairs. In addition to providing supporting evidence for Lcn2 binding partners, this approach can also reveal the occurrence of ligand-induced dimerization. The association of either ferric Ent or ferric 2,3-DHBA to Lcn2 was clearly marked by mass increases, as previously reported (Figure 2a−c).[22] However,

DOI: 10.1021/acschembio.9b00820
ACS Chem. Biol. 2020, 15, 234−242

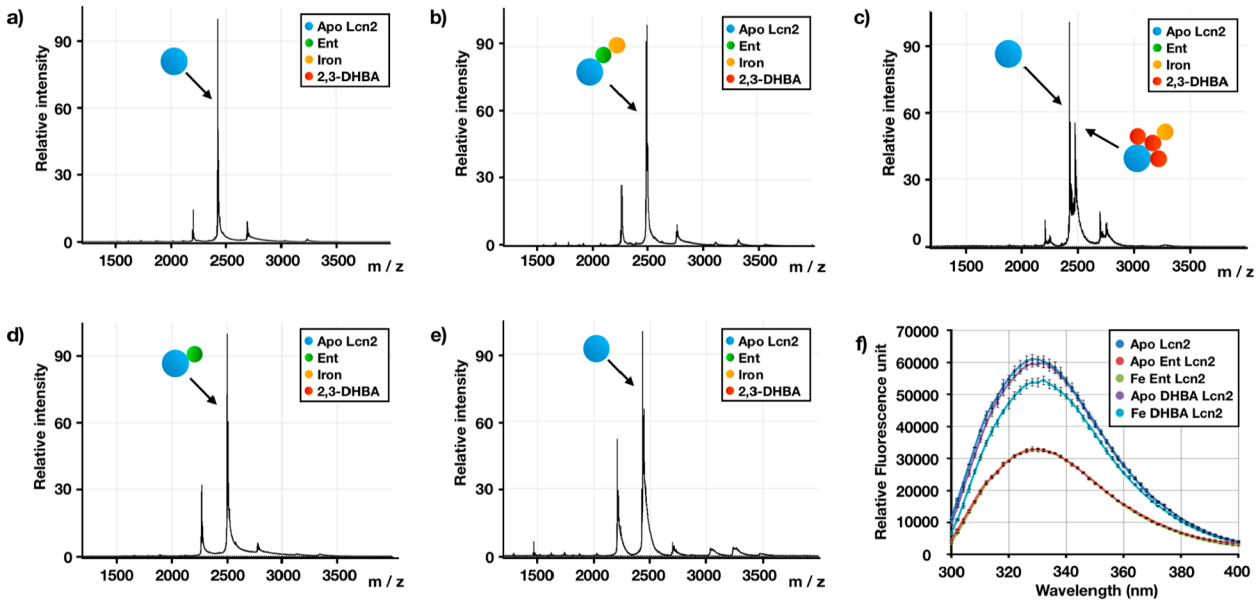

Figure 2. Formation of various siderophore−siderocalin complexes. Native MS spectra show the complexes formed when (a) free Lcn2 is incubated with (b) ferric enterobactin, (c) ferric 2,3-DHBA, (d) enterobactin, and (e) 2,3-DHBA. Spectra (a,b,c) were adapted with permission from Song et al.[22] (f) Fluorescence emission scans for the same complexes were collected from 300 to 400 nm when excited at 280 nm. Note that the Fe-Ent-Lcn2 and Apo-Ent-Lcn2 traces exhibit almost complete overlap.

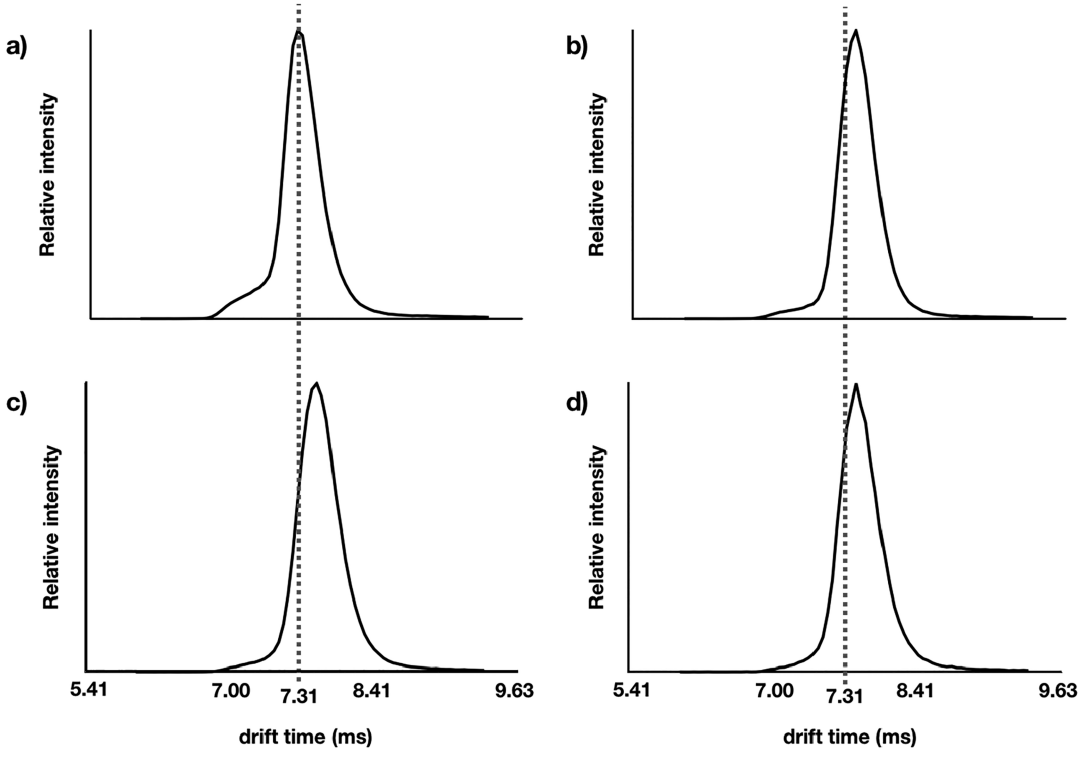

Figure 3. IMS chromatogram of various Lcn2-siderophore complexes. Corrected drift times were shown for complexes under the same conditions. The dotted line representing the peak centroid of (a) apo-Lcn2, is used as a reference line in (b) Lcn2-Ent, (c) Lcn2-Ent-Fe, and (d) Lcn2−2,3-DHBA-Fe chromatograms. All ligand-bound species showed longer drift times corresponding to less compact structures.

only Ent can bind to Lcn2 in the absence of iron (Figure 2d). The inability of Lcn2 to bind to 2,3-DHBA without iron is suggested via native MS (Figure 2e); however, this measurement is susceptible to false negatives (and false positives).[34] Since the barrel of Lcn2 is tyrosine-rich,[35] the emission spectrum of intrinsic fluorescence was used as a secondary measurement for Lcn2−siderophore interactions. Fluorescence intensity decreases were shown to occur upon addition of siderophore, consistent with binding in the calyx pocket (Figure 2f). This decrease was strongest for Ent and Ent-Fe, significant for 2,3-DHBA-Fe and was not measurable for 2,3-

DOI: 10.1021/acschembio.9b00820
ACS Chem. Biol. 2020, 15, 234−242

DHBA, showing in agreement with the MS data that 2,3-DHBA does not bind Lcn2 in the absence of iron (Figure 2f).

Apart from illustrating Lcn2 binding partners, the data in Figure 2 provide no evidence of substantial ligand-induced dimerization. Previously, covalent (disulfide) Lcn2 dimers in urine samples from patients with urinary tract infection had been observed.[32] However, the corresponding very low intensity peaks observed in the ESI mass spectrum are most likely artifactual (and noncovalent) dimers. Therefore, the second event indicated by the ITC measurements is not oligomerization.

Siderophore Binding Destabilizes the Native Structure of Lcn2. To test whether a folding/unfolding equilibrium disturbance was the second event measured by ITC, we examined the conformational changes of Lcn2 upon siderophore binding. IM-MS of the unbound protein revealed a single conformation with a drift time of 7.31 ± 0.03 ms (Figure 3a). Ligand-bound Lcn also exhibited a single conformational state, but all ligands induced a longer drift time compared to apo-Lcn2 (Figure 3b–d), signaling a larger collisional cross section. However, it is not clear if an increase of this magnitude, corresponding to 0.22 ± 0.04 ms, is a result of conformational change or a direct effect of the presence of ligand.

Global HDX measurements, which are specifically sensitive to changes in conformation and dynamics, revealed that siderophore-bound complexes uniformly exhibited higher deuterium uptake than the apoprotein (Figure 4). This is an

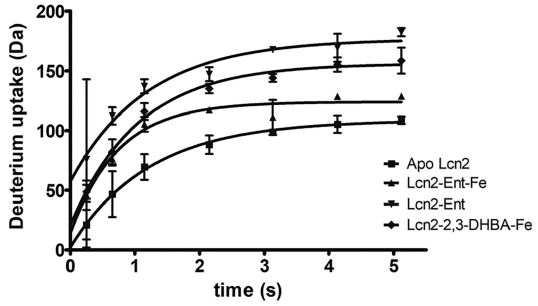

Figure 4. Global HDX from 0.25 to 5.12 s. The increases in mass after deuterium incorporation for the four Lcn2 states were plotted against HDX time, fitted with one phase association. Error bars from both technical ($n > 3$) and biological ($n \geq 3$) replicates were shown. The goodness of fit (R^2) are 0.97, 0.99, 0.96, 0.99 for Lcn2 alone, Ent-Fe bound, Ent bound, and three 2,3-DHBA-Fe bound Lcn2, respectively.

exceedingly unusual result since ligand binding typically induces decreased conformational dynamics (and thus lower deuterium uptake) through the formation of new structure-stabilizing interactions at the binding site. Nonetheless, structurally destabilizing interactions have been predicted to be hypothetically possible, with an example involving a modified heme ligand, in what Konermann et al. called a "Type II" scenario.[36] The structural distortion accompanied by accommodating ligands appears to be greater for siderophores with higher degrees of freedom. For instance, the binding of three 2,3-DHBA to an iron could be reckoned as flexible, as three catecholate units bind to iron in a hexa-dentate fashion. Iron-free Ent is also another example of a ligand with higher flexibility, where the partially flexible "arms" linking the catecholate groups potentially contribute to higher dynamics of the bound lipocalin (Figure S1).

Taken together, the IM-MS and global HDX data indicate a shift in the native Lcn2 folding landscape toward more dynamic/unfolded states, thus suggesting that protein unfolding is likely to be the second ITC event. To understand the nature of this conformational shift in detail, we employ structurally resolved HDX measurements.

The Structural Distortion Is Localized around the Lcn2 Calyx. To probe the disrupted region of Lcn2 after siderophore binding, we employed Time-Resolved ESI (TRESI) HDX, a "bottom up" approach in which HDX is quenched after a millisecond labeling period and the protein is digested prior to MS analysis.[37] Deuterium uptake values were summed across seven time points corresponding to 0.25–5.12 s. Ent-bound Lcn2 showed broad destabilization of the protein structure (red), but the greatest destabilization at the calyx around the three binding sites (128Y, 147K, 156K) predicted based on sequence homology from homo Lcn2[38] (Figure 5a, top panel). Like Ent, Ent-Fe also distorted Lcn2 at a similar region of the β barrel, albeit more selectively (Figure 5a, middle panel). The other iron-loaded siderophore, [2,3-DHBA]-Fe, exhibited the same destabilization of the calyx (albeit weaker) and the protective effect at the 3_{10} helix (Figure 5a, bottom panel). Even though the ferric 2,3-DHBA Lcn2 complex shows a lower magnitude of disruption for most peptides, the distortion might be more pronounced than the TRESI HDX difference amplitudes suggest. This is due to the presence of peptides from unbound Lcn2 in the sample which, based on the native MS data, may be uniquely present in the case of 2,3-DHBA-Fe. Under the short labeling conditions used here, uptake from peptides arising from the unbound protein will be averaged with uptake from the corresponding peptides arising from the bound protein, dampening the apparent difference. Lcn2 interacting with Ent is free from this complication since it is essentially saturated with ligand, as indicated by ESI-MS. At a longer exchange time point (e.g., 15 min), many of the differences across all three states are greatly subdued or no longer detected (Figure 5b).

To better understand the localized HDX results, the interaction between Lcn2 and Ent-Fe was modeled using protein–ligand docking by Molecular Operating Environment (MOE).[39] The amino acids involved in the Ent-Fe/Lcn2 interaction are shown schematically, colored based on the different types of interactions, in Figure 6a. The orientation of Ent-Fe inside the calyx is shown as a cartoon representation (Figure 6b). As expected, the iron atom in this structure is chelated with three bidentate catecholates of enterobactin (shown in black), in which the catechol oxygen atoms of the 2,3-DHBA moieties make a hexa-coordinate octahedral complex with Fe(III).

The increases in dynamics are not only observed at the binding site but spread across the calyx. The distortion of the protein structure corroborates well with the Ent/Lcn2 interaction surface illustrated by docking poses produced by MOE. The docking pose represented in Figure 6 does not give any additional information on protective effects at the 3_{10} helix (aa 112–129) for the 2,3-DHBA-Fe moiety.

Taken together, our results indicate that siderophores interact with Lcn2 in a noncanonical way that involves destabilization of the protein structure. Though rare, the stabilization of partially unfolded states of a protein upon ligand binding has been previously reported. $NADP^+$, for instance, has been shown to prolong the lifetime of unfolding intermediates of dihydrofolate reductase.[40,41] Similarly, 1,8-

DOI: 10.1021/acschembio.9b00820
ACS Chem. Biol. 2020, 15, 234–242

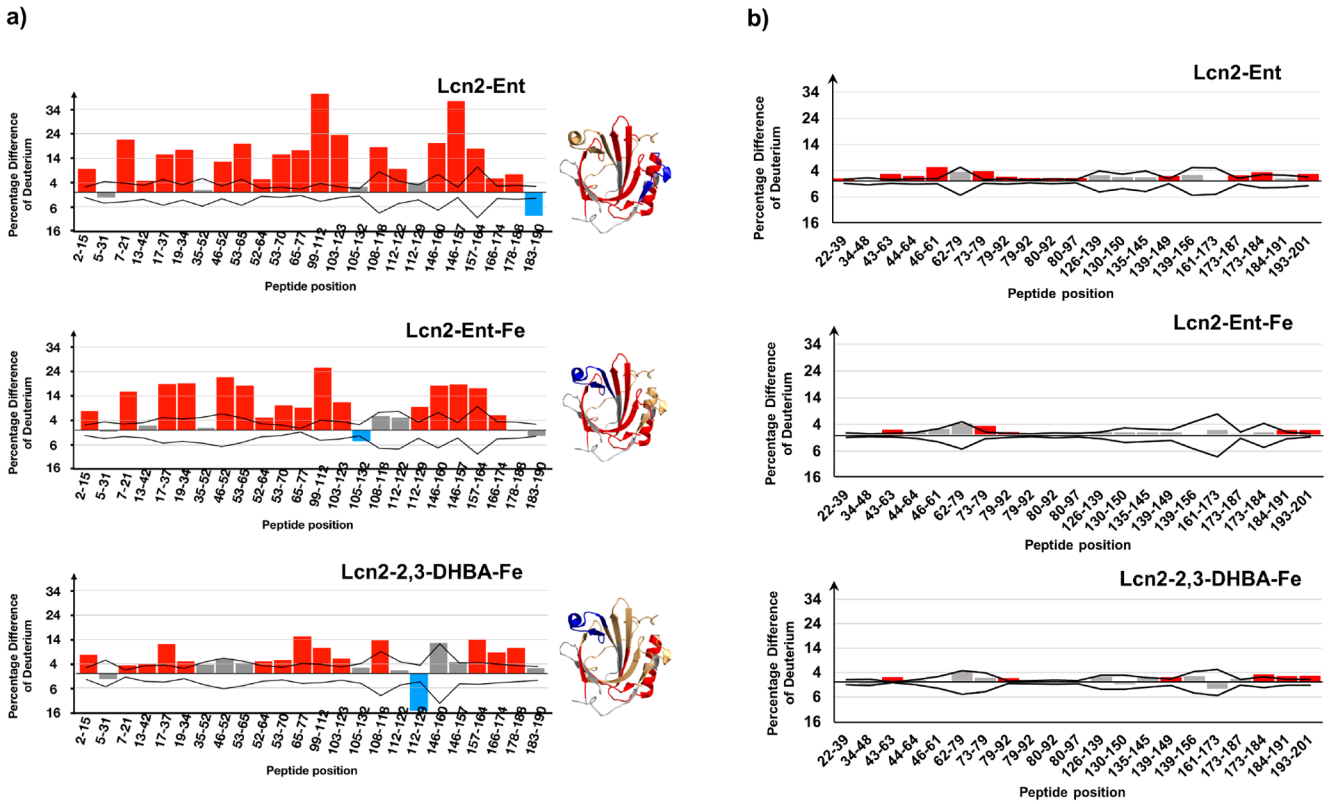

Figure 5. Difference plots of local HDX data. The difference in deuterium uptake of (a) enterobactin loaded, ferric enterobactin loaded, and ferric 2,3-DHBA loaded compared to apo Lcn2. Significant increases after binding are plotted in red and decreases are plotted in blue. Regions with nonsignificant differences are colored in gold, while gray areas represent the regions with no sequence coverage. Deuterium uptake values were summed across seven time points corresponding to 0.25−5.12 s. (b) Difference plots of all three states at a single time point corresponding to 15 min. The statistical significance threshold (2σ, $n = 3$) is given by the black line that runs through the bar plot. Only differences greater than this threshold are included.

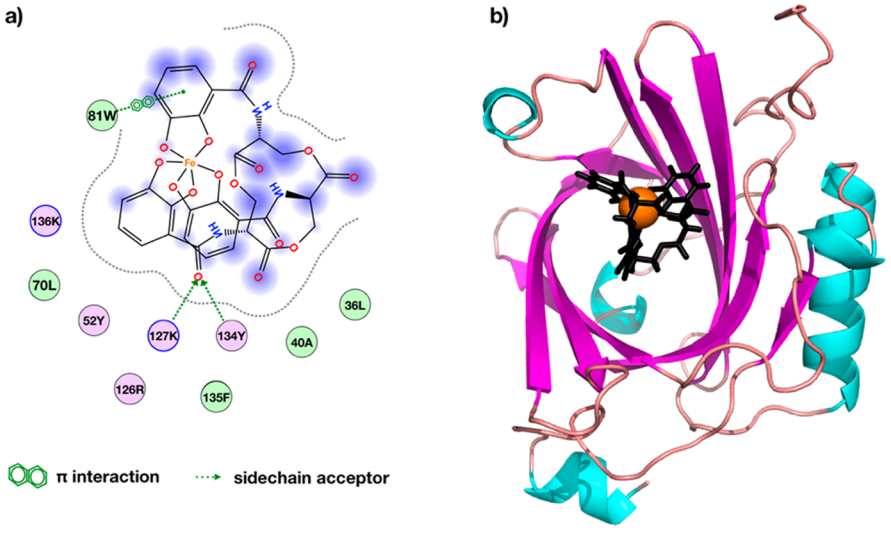

Figure 6. Ferric Ent docked to Lcn2 by MOE simulation. (a) Amino acids involved in ferric Ent binding are shown as schematic representations, where 81W, 127K, and 134Y are in direct interaction with the siderophore. Structure of deprotonated $[(Ent)Fe(III)]^{3-}$ at pH 7 is used for the docking process. (b) Cartoon representation, colored by secondary structures, reveals the position of the ligand docked at the calyx.

anilinonaphthalenesulfonate facilitates unfolding of the Polo-box domain of Polo-like kinase 1, and zinc destabilizes the structure of porcine growth hormone.[42] A thermodynamic model for such interactions was provided by Konermann et al.[36] In the case of Lcn2, where both binding processes are favorable (based on ITC), the enthalpic penalty for increased conformational flexibility might get "paid" by release of ordered water within the calyx, but we have not found direct evidence of this. The conformational distortion can also be potentially crucial for downstream Lcn2 function, such as iron

DOI: 10.1021/acschembio.9b00820
ACS Chem. Biol. 2020, 15, 234−242

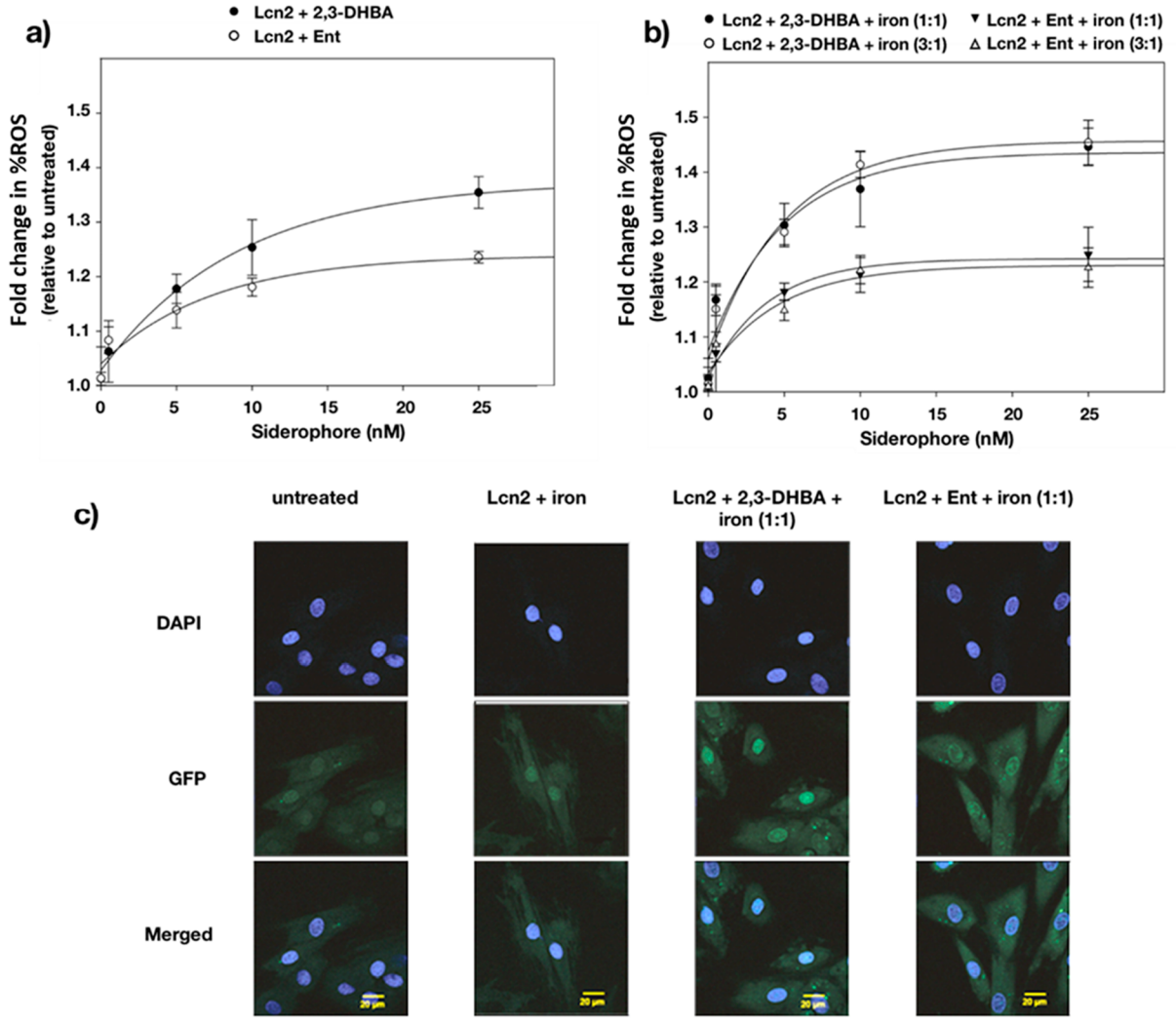

Figure 7. Intracellular ROS level changes responding to holo-Lcn2 treatment. The dose-dependent fold change of ROS production was measured with ferric 2,3-DHBA or Ent, with (a) trace iron in full media or (b) supplementary iron. (c) The representative fluorescence cell images for two controls, untreated H9C2 cells, and treated with Lcn2 and iron, are shown on the left side. The increase in green fluorescence intensity is from cells treated with 10 nM siderophore concentration at a ratio of 1:1 siderophore-iron. DAPI was used as reference fluorescence for the nucleus. Error bars are from three biological replicates (n = 3).

and siderophore influx by facilitating a more favorable interaction with receptors mediating the endocytosis.

Ferric 2,3-DHBA Induces More Cellular Toxicity than Ferric Ent. The effect of iron-loaded Lcn2 on ROS production was tested in H9C2 cells. Relying solely on trace amounts of iron in complete growth media, 2,3-DHBA treated cells had a higher ROS response than the Ent treated group (Figure 7a). Because ferric 2,3-DHBA formed a complex with Lcn2 at a ratio of 1:3:1 Lcn2:2,3-DHBA:iron, equivalent and 1/3 iron concentrations were used to conduct subsequent experiments. With an intentional iron supplement, ferric 2,3-DHBA treatment has a significantly higher ROS response than the ferric Ent group. However, this appears to correlate to a different saturation point as increasing iron concentrations had no effect (Figure 7b). Representative cell fluorescence images and their quantitative analysis clearly illustrated that iron-laden 2,3-DHBA Lcn2 complex treated cells had greater level of ROS (Figure 7c). Apo-Lcn2 or Lcn2 with iron alone did not cause significant ROS accumulation compared to untreated cells.

Higher ROS levels are observed with ferric 2,3-DHBA than with ferric Ent at the same concentration. This can be rationalized from the molecular data in that the increased conformational distortion associated with 2,3-DHBA-Fe binding could be more susceptible to siderophore loss in endosomes. Apo-Lcn2 has been shown to be highly resistant to unfolding, even at pH 2.5, but the ligand-bound form appears to unfold more readily in response to lowered pH, increasing the likelihood of siderophore release.[22] It has recently been demonstrated that Ent-Fe binds to ATP synthase subunit α inside mitochondria and facilitates iron influx; this provides a possible destination for Ent-Fe.[5] Ultimately, our work reveals that an unusual, structurally destabilizing interaction between Lcn2 and its iron-loaded siderophores may be the molecular origin of Lcn2-mediated inflammation.

The "strained" nature of this interaction, together with its widespread expression in the absence of bacterial infection, suggests that Lcn2's role in the innate immune response may represent an example of molecular exaptation. Specifically, Lcn2 may have originally evolved to fill a role in line with other

DOI: 10.1021/acschembio.9b00820
ACS Chem. Biol. 2020, 15, 234−242

lipocalins (i.e., lipid transport), but was later selected for overexpression in bacterial infection to sequester bacterial siderophores. Lcn2 is therefore imperfectly suited to the latter role in the sense that, having not evolved specifically to bind siderophore targets, complexation requires substantial distortion of the binding pocket resulting in an elevated probability of releasing ferric siderophore from endosomes. In the case of bacterial infection, where Ent-Fe is abundant, the benefits of iron chelation outweigh the cost of free intracellular ferric siderophore (and moderately elevated ROS production). However, when Lcn2 is expressed in the absence of infection, there is no significant benefit of iron chelation, and the higher distortion interaction with 2,3-DHBA-Fe results in substantially elevated ROS production leading to adverse biological effects contributing to various disease pathophysiologies. A detailed functional evolution analysis of the Lcn protein family could provide insights into this hypothesis and is a target for future work.

METHODS

Reagents. All reagents were purchased from Sigma-Aldrich unless otherwise stated. Ni Sepharose 6 Fast Flow resin was purchased from GE Healthcare Life Sciences. Dialysis cassettes were purchased from Thermo Fisher Scientific.

Protein Expression and Purification. pPROEX HTb murine Lipocalin-2 was expressed in *E. coli* BL21 and purified using Ni Sepharose 6 Fast Flow resin as we previously described.[43,44] Subsequently, the protein was dialyzed into 1× PBS (137 mM NaCl, 2.7 mM KCl, 10 mM Na_2HPO_4, 1.76 KH_2PO_4, pH 7.4) for long-term storage.

Lcn2 Siderophore Interactions. Molecules 2,3-DHBA and Ent were dissolved in DMSO at concentrations of 300 mM and 15 mM, respectively. Ratios of Lcn2:2,3-DHBA (1:3) or Lcn2:Ent (1:1) were used to form the complexes. When iron was involved, $FeCl_3$ was premixed with siderophores before addition into Lcn2.

Isothermal Titration Calorimetry (ITC). ITC was performed using a MicroCal VP-ITC. Samples were degassed before analysis with a MicroCal Thermo Vac unit. Titrations were performed with the protein sample in the cell and the siderophore as the titrant. The binding experiments were performed at 20 °C with 0.25 mM Ent and 12 μM or 40 μM Lcn2. Siderophore, initially dissolved in 100% DMSO, was diluted to working concentrations with 1× PBS (pH 7.4) buffer to a final DMSO concentration of 0.56% (v/v). DMSO was added to the protein solution and the reference cell at the same concentration to avoid buffer mismatch. All binding experiments consisted of the first injection of 2 mL and a 60 s delay. The subsequent 34 injections were 8 mL, spaced every 300 s. The first point was removed prior to analysis due to the different injection volume and delay parameters. ITC binding data were fit to a sequential binding model developed by Freiburger et al.[45] using Matlab 14 software.

Native and Ion Mobility Mass Spectrometry. The Lcn2-siderophore complexes were identified at 5 μM Lcn2 in 100 mM NH_4Ac (pH 6.8) by ESI mass spectrometry (Waters Synapt G2-S). The instrument was operated in positive ion mode with 2.5 kV source voltage and 30 V sampling cone. Trap and transfer collision energy were set to 5 and 10 eV, respectively. When ion mobility was used to characterize the different complexes, traveling wave was set to 600 m/s velocity and 30 V height. IMS cell was filled with nitrogen gas flowing at 90 mL/min, giving a pressure of 0.319 mbar. The drift time was corrected with a calibration curve created using a literature cross-collisional section of cytochrome c, ubiquitin, and myoglobin.[46]

Intrinsic Fluorescence Emission Spectra. Apo-Lcn2 or siderophore-siderocalin complexes were prepared at 5 μM in 1× PBS as described above. The samples were excited at a wavelength of 280 nm (bandwidth 9 nm). The emission fluorescence was measured on Synergy H4 (BioTek), operated by Gen5. The emission spectra were collected at a 2 nm interval over the 300−400 nm range at 22 °C.

Global and Local HDX of Lcn2. The microfluidic setup for HDX experiments was assembled as previously described.[47,48] Briefly, HDX took place in a Time-Resolved ElectroSpray Ionization (TRESI) mixer, allowing for various reaction times. In the global HDX set up, labeled protein solution was sprayed into the mass spectrometer directly following mixing. Based on flow rates of 5 μL/min protein and 10 μL/min deuterium, seven time points were collected from 0.25 to 5.12 s. In the local HDX set up, deuterated protein was quenched with 10% acetic acid and 5% acetonitrile before online digestion in a PMMA chip with pepsin and protease XIII linked agarose beads.[48] With protein and deuterium flow rates each at 2 μL/min, the HDX reaction times were calculated to be 0.68 and 3.4 s.

HDX Data Analysis. The deuterium incorporation in global HDX was calculated based on deconvoluted masses from multiple charge states before and after the HDX reaction. For TRESI-HDX experiments, peptides were identified by the ExPASy FindPept tool. Peptides with multiple sequence matches were further confirmed by MS/MS. Upon generation of the peptide list, deuterium uptake levels were calculated by Mass Spec Studio.[49] Differences of the deuterium uptake between the complex and apo Lcn2 were reported. The summed deuterium uptakes for all time points were reported.

Molecular Operating Environment (MOE) Simulation. All the docking and Loop Modeling calculations were performed using MOE 2018.0101 software. The crystal structure of murine Lcn2 was taken from Protein Data Bank (PDB 3S26).[50] This structure was missing secondary structural information for four segments in the sequence, i.e., QDSTQ, TEG, DQDQ, and AWSHPQFEK. The structures of these missing loops were modeled using the "Loop Modeler" utility provided in MOE software with the default settings. The active site of the protein was found using the "Site Finder" option in MOE. Site Finder used a geometrical method (Alpha Spheres) to exclude the regions too exposed to solvent or too packed,[51,52] and then scores the accepted regions by the hydrophobic interactions. As a result, the ferric Ent could be conveniently docked to the calyx, by using the dummy atoms acquired by "Site Finder". The optimized structure of the ferric Ent was retrieved from Johnstone et al., which was equivalent to their crystallographic structure.[53] A side-chains tethered semirigid protocol, with a restraining potential of 10 kcal/mol, was taken in the docking process. Ligand placement and rescoring were performed by Triangle Matcher and London ΔG method, respectively. Five hundred poses were produced. The top pose having the highest score was taken.

ROS Detection in H9C2 Cells by DCF-DA Assay. H9C2 cells were treated with various concentrations (0−25 nM) of 2,3-DHBA or Ent in the presence of Lcn2/iron and incubated with 20 μM MDCF-DA (DC-FDA; Sigma-Aldrich) for 2 h (three cultures per condition). DCF-DA is cleaved by ROS to generate a highly fluorescent 2′,7′-dichlorofluorescein (DCF) molecule, which was measured at 490/530 nm by a Synergy H4 multimode plate reader (BioTek).

ROS Determination by CellROXGreen Assay. H9C2 cells attached to coverslips were treated for 2 h with various concentrations (0−25 nM) of 2,3-DHBA or Ent in the presence of Lcn2/iron (three cultures per condition). CellROXGreen (2.5 μM) was added into the medium 15 min before further processing. The coverslips were washed immediately by chilled 1× PBS twice before paraformaldehyde fixation. After quenching with 1% glycine for 10 min, the coverslips were mounted with a mixture of ProLong Gold Antifade and DAPI (3:1). Images were taken at 1024 × 1024 resolution by a Zeiss LSM 700 40× oil immersion objective.

ASSOCIATED CONTENT

Supporting Information

The Supporting Information is available free of charge on the ACS Publications website at DOI: 10.1021/acschembio.9b00820.

Schematic structures for 2,3-DHBA and iron-free Enterobactin (PDF)

DOI: 10.1021/acschembio.9b00820
ACS Chem. Biol. 2020, 15, 234−242

AUTHOR INFORMATION

Corresponding Author

*E-mail: dkwilson@yorku.ca.

ORCID

Philip E. Johnson: 0000-0002-5573-4891

Derek J. Wilson: 0000-0002-7012-6085

Funding

This work is supported by the Natural Sciences and Engineering Research Council of Canada (NSERC) Discovery (504027), Engage (492095-15), and Collaborative Research and Development (CRD) (485321-15) programs. G.S. acknowledges support via a Grant-in-aid and Career Investigator Award from Heart & Stroke Foundation of Canada.

Notes

The authors declare no competing financial interest.

REFERENCES

(1) Kjeldsen, L., Cowland, J. B., and Borregaard, N. (2000) Human Neutrophil Gelatinase-Associated Lipocalin and Homologous Proteins in Rat and Mouse. *Biochim. Biophys. Acta, Protein Struct. Mol. Enzymol. 1482*, 272−283.

(2) Friedl, A., Stoesz, S. P., Buckley, P., and Gould, M. N. (1999) Neutrophil Gelatinase-Associated Lipocalin in Normal and Neoplastic Human Tissues. Cell Type-Specific Pattern of Expression. *Histochem. J. 31*, 433−441.

(3) Xu, G., Ahn, J., Chang, S., Eguchi, M., Ogier, A., Han, S., Park, Y., Shim, C., Jang, Y., Yang, B., et al. (2012) Lipocalin-2 Induces Cardiomyocyte Apoptosis by Increasing Intracellular Iron Accumulation. *J. Biol. Chem. 287*, 4808−4817.

(4) Jang, Y., Lee, J. H., Wang, Y., and Sweeney, G. (2012) Emerging Clinical and Experimental Evidence for the Role of Lipocalin-2 in Metabolic Syndrome. *Clin. Exp. Pharmacol. Physiol. 39*, 194−199.

(5) Qi, B., and Han, M. (2018) Microbial Siderophore Enterobactin Promotes Mitochondrial Iron Uptake and Development of the Host via Interaction with ATP Synthase. *Cell 175*, 571−582.

(6) Chu, S. T., Lin, H. J., Huang, H. L., and Chen, Y. H. (1998) The Hydrophobic Pocket of 24p3 Protein from Mouse Uterine Luminal Fluid: Fatty Acid and Retinol Binding Activity and Predicted Structural Similarity to Lipocalins. *J. Pept. Res. 52*, 390−397.

(7) Goetz, D. H., Willie, S. T., Armen, R. S., Bratt, T., Borregaard, N., and Strong, R. K. (2000) Ligand Preference Inferred from the Structure of Neutrophil Gelatinase Associated Lipocalin. *Biochemistry 39*, 1935−1941.

(8) Flower, D. R. (1996) The Lipocalin Protein Family: Structure and Function. *Biochem. J. 318*, 1−14.

(9) Bratt, T., Ohlson, S., and Borregaard, N. (1999) Interactions between Neutrophil Gelatinase-Associated Lipocalin and Natural Lipophilic Ligands. *Biochim. Biophys. Acta, Gen. Subj. 1472*, 262−269.

(10) Goetz, D. H., Holmes, M. A., Borregaard, N., Bluhm, M. E., Raymond, K. N., and Strong, R. K. (2002) The Neutrophil Lipocalin NGAL Is a Bacteriostatic Agent That Interferes with Siderophore-Mediated Iron Acquisition. *Mol. Cell 10*, 1033−1043.

(11) Bachman, M. A., Miller, V. L., and Weiser, J. N. (2009) Mucosal Lipocalin 2 Has Pro-Inflammatory and Iron-Sequestering Effects in Response to Bacterial Enterobactin. *PLoS Pathog. 5* (10), No. e1000622.

(12) Berger, T., Togawa, A., Duncan, G. S., Elia, A. J., You-Ten, A., Wakeham, A., Fong, H. E. H., Cheung, C. C., and Mak, T. W. (2006) Lipocalin 2-Deficient Mice Exhibit Increased Sensitivity to Escherichia Coli Infection but Not to Ischemia-Reperfusion Injury. *Proc. Natl. Acad. Sci. U. S. A. 103*, 1834−1839.

(13) Singh, V., Yeoh, B. S., Chassaing, B., Zhang, B., Saha, P., Xiao, X., Awasthi, D., Shashidharamurthy, R., Dikshit, M., Gewirtz, A., et al. (2016) Microbiota-Inducible Innate Immune, Siderophore Binding Protein Lipocalin 2 Is Critical for Intestinal Homeostasis. *Cell. Mol. Gastroenterol. Hepatol. 2*, 482−498.

(14) Bao, G., Clifton, M., Hoette, T. M., Mori, K., Deng, S.-X., Qiu, A., Viltard, M., Williams, D., Paragas, N., Leete, T., et al. (2010) Iron Traffics in Circulation Bound to a Siderocalin (Ngal)-Catechol Complex. *Nat. Chem. Biol. 6*, 602−609.

(15) Toyonaga, T., Matsuura, M., Mori, K., Honzawa, Y., Minami, N., Yamada, S., Kobayashi, T., Hibi, T., and Nakase, H. (2016) Lipocalin 2 Prevents Intestinal Inflammation by Enhancing Phagocytic Bacterial Clearance in Macrophages. *Sci. Rep. 6*, 35014.

(16) Yan, Q.-W., Yang, Q., Mody, N., Graham, T. E., Hsu, C.-H., Xu, Z., Houstis, N. E., Kahn, B. B., and Rosen, E. D. (2007) The Adipokine Lipocalin 2 Is Regulated by Obesity and Promotes Insulin Resistance. *Diabetes 56*, 2533−2540.

(17) Naudé, P. J. W., Nyakas, C., Eiden, L. E., Ait-Ali, D., van der Heide, R., Engelborghs, S., Luiten, P. G. M., De Deyn, P. P., den Boer, J. A., and Eisel, U. L. M. (2012) Lipocalin 2: Novel Component of Proinflammatory Signaling in Alzheimer's Disease. *FASEB J. 26*, 2811−2823.

(18) Pereira, S. S., and Alvarez-Leite, J. I. (2014) Low-Grade Inflammation, Obesity, and Diabetes. *Curr. Obes. Rep. 3*, 422−431.

(19) Zhao, P., Elks, C. M., and Stephens, J. M. (2014) The Induction of Lipocalin-2 Protein Expression in Vivo and in Vitro. *J. Biol. Chem. 289*, 5960−5969.

(20) Iannetti, A., Pacifico, F., Acquaviva, R., Lavorgna, A., Crescenzi, E., Vascotto, C., Tell, G., Salzano, A. M., Scaloni, A., Vuttariello, E., et al. (2008) The Neutrophil Gelatinase-Associated Lipocalin (NGAL), a NF-KappaB-Regulated Gene, Is a Survival Factor for Thyroid Neoplastic Cells. *Proc. Natl. Acad. Sci. U. S. A. 105*, 14058−14063.

(21) Lee, S., Lee, J., Kim, S., Park, J.-Y., Lee, W.-H., Mori, K., Kim, S.-H., Kim, I. K., and Suk, K. (2007) A Dual Role of Lipocalin 2 in the Apoptosis and Deramification of Activated Microglia. *J. Immunol. 179*, 3231−3241.

(22) Song, E., Ramos, S. V., Huang, X., Liu, Y., Botta, A., Sung, H. K., Turnbull, P. C., Wheeler, M. B., Berger, T., Wilson, D. J., et al. (2018) Holo-Lipocalin-2-Derived Siderophores Increase Mitochondrial ROS and Impair Oxidative Phosphorylation in Rat Cardiomyocytes. *Proc. Natl. Acad. Sci. U. S. A. 115*, 1576−1581.

(23) Guo, B.-X., Wang, Q.-Q., Li, J.-H., Gan, Z.-S., Zhang, X.-F., Wang, Y.-Z., and Du, H.-H. (2017) Lipocalin 2 Regulates Intestine Bacterial Survival by Interplaying with Siderophore in a Weaned Piglet Model of Escherichia Coli Infection. *Oncotarget 8*, 65386−65396.

(24) Xiao, X., Yeoh, B. S., and Vijay-Kumar, M. (2017) Lipocalin 2: An Emerging Player in Iron Homeostasis and Inflammation. *Annu. Rev. Nutr. 37*, 103−130.

(25) Abella, V., Scotece, M., Conde, J., Gómez, R., Lois, A., Pino, J., Gómez-Reino, J. J., Lago, F., Mobasheri, A., and Gualillo, O. (2015) The Potential of Lipocalin-2/NGAL as Biomarker for Inflammatory and Metabolic Diseases. *Biomarkers 20*, 565−571.

(26) Banjara, M. (2014) Lipocalin-2: A New Regulator of Non-Pathogen-Associated Neuroinflammation. *Int. J. Clin. Exp. Neurol. 2*, 8−15.

(27) Brown, A. (2009) Analysis of Cooperativity by Isothermal Titration Calorimetry. *Int. J. Mol. Sci. 10*, 3457−3477.

(28) Brautigam, C. A. (2015) Fitting Two- and Three-Site Binding Models to Isothermal Titration Calorimetric Data. *Methods 76*, 124−136.

(29) Kovriguine, E. (2017) Resolving Three-State Ligand-Binding Mechanisms By Isothermal Titration Calorimetry: A Simulation Study, *BioRxiv Beta*.

(30) Shrake, A., and Ross, P. D. (1990) Ligand-Induced Biphasic Protein Denaturation. *J. Biol. Chem. 265*, 5055−5059.

(31) Seo, M.-H., Park, J., Kim, E., Hohng, S., and Kim, H.-S. (2014) Protein Conformational Dynamics Dictate the Binding Affinity for a Ligand. *Nat. Commun. 5*, 3724.

DOI: 10.1021/acschembio.9b00820
ACS Chem. Biol. 2020, 15, 234−242

(32) Cai, L., Rubin, J., Han, W., Venge, P., and Xu, S. (2010) The Origin of Multiple Molecular Forms in Urine of HNL/NGAL. *Clin. J. Am. Soc. Nephrol. 5*, 2229−2235.
(33) Strong, R. K., Bratt, T., Cowland, J. B., Borregaard, N., Wiberg, F. C., and Ewald, A. J. (1998) Expression, Purification, Crystallization and Crystallographic Characterization of Dimeric and Monomeric Human Neutrophil Gelatinase Associated Lipocalin (NGAL). *Acta Crystallogr., Sect. D: Biol. Crystallogr. 54*, 93−95.
(34) Sun, J., Kitova, E. N., Wang, W., and Klassen, J. S. (2006) Method for Distinguishing Specific from Nonspecific Protein-Ligand Complexes in Nanoelectrospray Ionization Mass Spectrometry. *Anal. Chem. 78*, 3010−3018.
(35) Ruan, K., Li, J., Liang, R., Xu, C., Yu, Y., Lange, R., and Balny, C. (2002) A Rare Protein Fluorescence Behavior Where the Emission Is Dominated by Tyrosine: Case of the 33-KDa Protein from Spinach Photosystem II. *Biochem. Biophys. Res. Commun. 293*, 593−597.
(36) Konermann, L., Rodriguez, A. D., and Sowole, M. A. (2014) Type 1 and Type 2 Scenarios in Hydrogen Exchange Mass Spectrometry Studies on Protein-Ligand Complexes. *Analyst 139*, 6078−6087.
(37) Rob, T., Liuni, P., Gill, P. K., Zhu, S., Balachandran, N., Berti, P. J., and Wilson, D. J. (2012) Measuring Dynamics in Weakly Structured Regions of Proteins Using Microfluidics-Enabled Subsecond H/D Exchange Mass Spectrometry. *Anal. Chem. 84*, 3771−3779.
(38) Bateman, A., Martin, M. J., O'Donovan, C., Magrane, M., Alpi, E., Antunes, R., Bely, B., Bingley, M., Bonilla, C., Britto, R., et al. (2017) UniProt: The Universal Protein Knowledgebase. *Nucleic Acids Res. 45* (D1), D158−D169.
(39) *Molecular Operating Environment (MOE)*, Chemical Computing Group ULC, 1010 Sherbrooke St. West, Suite #910, Montreal, QC, Canada, H3A 2R7, 2019.
(40) Kasper, J. R., and Park, C. (2015) Ligand Binding to a High-Energy Partially Unfolded Protein. *Protein Sci. Publ. Protein Soc. 24*, 129−137.
(41) Junker, J. P., Hell, K., Schlierf, M., Neupert, W., and Rief, M. (2005) Influence of Substrate Binding on the Mechanical Stability of Mouse Dihydrofolate Reductase. *Biophys. J. 89*, L46−L48.
(42) Cimmperman, P., Baranauskiene, L., Jachimoviciūte, S., Jachno, J., Torresan, J., Michailoviene, V., Matuliene, J., Sereikaite, J., Bumelis, V., and Matulis, D. (2008) A Quantitative Model of Thermal Stabilization and Destabilization of Proteins by Ligands. *Biophys. J. 95*, 3222−3231.
(43) Wang, Y., Xu, A., Knight, C., Xu, L. Y., and Cooper, G. J. S. (2002) Hydroxylation and Glycosylation of the Four Conserved Lysine Residues in the Collagenous Domain of Adiponectin POTENTIAL ROLE IN THE MODULATION OF ITS INSULIN-SENSITIZING ACTIVITY. *J. Biol. Chem. 277*, 19521−19529.
(44) Wang, Y., Lam, K. S. L., Kraegen, E. W., Sweeney, G., Zhang, J., Tso, A. W. K., Chow, W.-S., Wat, N. M. S., Xu, J. Y., Hoo, R. L. C., et al. (2006) Lipocalin-2 Is an Inflammatory Marker Closely Associated with Obesity, Insulin Resistance, and Hyperglycemia in Humans. *Clin. Chem. 53*, 34−41.
(45) Freiburger, L. A., Auclair, K., and Mittermaier, A. K. (2009) Elucidating Protein Binding Mechanisms by Variable-c ITC. *ChemBioChem 10*, 2871−2873.
(46) Michaelevski, I., Kirshenbaum, N., and Sharon, M. (2010) T-Wave Ion Mobility-Mass Spectrometry: Basic Experimental Procedures for Protein Complex Analysis, *J. Visualized Exp.*, Issue 41, DOI: 10.3791/1985.
(47) Rob, T., and Wilson, D. J. (2009) A Versatile Microfluidic Chip for Millisecond Time-Scale Kinetic Studies by Electrospray Mass Spectrometry. *J. Am. Soc. Mass Spectrom. 20*, 124−130.
(48) Knox, R., Lento, C., and Wilson, D. J. (2018) Mapping Conformational Dynamics to Individual Steps in the TEM-1 β-Lactamase Catalytic Mechanism. *J. Mol. Biol. 430*, 3311−3322.
(49) Rey, M., Sarpe, V., Burns, K. M., Buse, J., Baker, C. A. H., van Dijk, M., Wordeman, L., Bonvin, A. M. J. J., and Schriemer, D. C. (2014) Mass Spec Studio for Integrative Structural Biology. *Structure 22*, 1538−1548.
(50) Bandaranayake, A. D., Correnti, C., Ryu, B. Y., Brault, M., Strong, R. K., and Rawlings, D. J. (2011) Daedalus: A Robust, Turnkey Platform for Rapid Production of Decigram Quantities of Active Recombinant Proteins in Human Cell Lines Using Novel Lentiviral Vectors. *Nucleic Acids Res. 39*, No. e143.
(51) Edelsbrunner, H., Facello, M., Fu, P., and Liang, J. (1995) Measuring Proteins and Voids in Proteins. *In Proceedings of the Twenty-Eighth Annual Hawaii International Conference on System Sciences 5*, 256−264.
(52) Liang, J., Edelsbrunner, H., and Woodward, C. (1998) Anatomy of Protein Pockets and Cavities: Measurement of Binding Site Geometry and Implications for Ligand Design. *Protein Sci. 7*, 1884−1897.
(53) Johnstone, T. C., and Nolan, E. M. (2017) Determination of the Molecular Structures of Ferric Enterobactin and Ferric Enantioenterobactin Using Racemic Crystallography. *J. Am. Chem. Soc. 139*, 15245−15250.

DOI: 10.1021/acschembio.9b00820
ACS Chem. Biol. 2020, 15, 234−242